Synthetic routes contaminate graphene materials with a whole spectrum of unanticipated metallic elements

Colin Hong An Wong[a], Zdeněk Sofer[b], Marie Kubešová[c], Jan Kučera[c], Stanislava Matějková[d], and Martin Pumera[a,1]

[a]Division of Chemistry and Biological Chemistry, School of Physical and Mathematical Sciences, Nanyang Technological University, Singapore 637371; [b]Department of Inorganic Chemistry, Institute of Chemical Technology, 166 28 Prague 6, Czech Republic; [c]Department of Nuclear Spectroscopy, Nuclear Physics Institute of the Academy of Sciences of the Czech Republic, 250 68 Řež, Czech Republic; and [d]Central Analytical Laboratory, Institute of Organic Chemistry and Biochemistry of the Academy of Sciences of the Czech Republic, 166 10 Prague 6, Czech Republic

Edited by Alexis T. Bell, University of California, Berkeley, CA, and approved August 18, 2014 (received for review July 15, 2014)

The synthesis of graphene materials is typically carried out by oxidizing graphite to graphite oxide followed by a reduction process. Numerous methods exist for both the oxidation and reduction steps, which causes unpredictable contamination from metallic impurities into the final material. These impurities are known to have considerable impact on the properties of graphene materials. We synthesized several reduced graphene oxides from extremely pure graphite using several popular oxidation and reduction methods and tracked the concentrations of metallic impurities at each stage of synthesis. We show that different combinations of oxidation and reduction introduce varying types as well as amounts of metallic elements into the graphene materials, and their origin can be traced to impurities within the chemical reagents used during synthesis. These metallic impurities are able to alter the graphene materials' electrochemical properties significantly and have wide-reaching implications on the potential applications of graphene materials.

The isolation of graphene nearly a decade ago has unleashed an immense wave of research into the field, revealing many of its exceptional mechanical, physical, and chemical properties (1, 2). Subsequently, a slew of potential applications for graphene have been suggested, ranging from electrosensing (3), sustainable energy production and storage (4–6), novel composites (7), and healthcare (8, 9) to electronics (10). These applications were based primarily on theoretical and experimental studies on pristine graphene [that is, a single layer "polycyclic aromatic hydrocarbon of quasi infinite size" without defects in the carbon sp^2 plane (11)]. Although the large-scale fabrication of pristine graphene is not yet a reality, various methods have been developed to synthesize graphitic carbon materials that closely approach the properties of pristine graphene. One such route involves the initial oxidation of graphite to graphite oxide (GO) followed by its reduction to yield reduced graphene oxide (RGO). Recently, the oxidative procedure has been successfully scaled up to industrial levels using a continuous stirred tank reactor process capable of yielding 2 kg GO per day from a single setup (12). The RGO subsequently obtained showed excellent electrical conductivity and surface area on par with RGO synthesized using more controlled laboratory procedures.

Several conditions and reagents for the oxidation of graphite to GO have been studied, which can be broadly classified as chlorate-based [the methods by Brodie (13), Staudenmaier (14), Hofmann and König (15), and Hofmann and Holst (16)] or permanganate-based [the method by Hummers and Offeman (17)]. The Hummers approach is the most commonly used procedure today to obtain GO, although many variations with small modifications exist. For the reduction step, methods available encompass thermal annealing, electrochemical reduction (18), irradiation (19), and chemical reduction. The last category itself is highly varied, using a plethora of traditional reducing agents, such as hydrazine (20), sodium borohydride (21), and lithium aluminum hydride (22); more unconventional greener agents, like reducing sugars (23) and tea solution (24), have been used as well. The wide selection of oxidizing and reducing agents offers practically unlimited combinations of procedures to synthesize RGOs from graphite, with large differences in the RGO material properties in each case (24).

The presence of residual metallic impurities in graphene is a known problem, and many of these impurities are able to dramatically alter the electronic and electrochemical properties of graphene (26–28). It is often falsely assumed in the graphene community that these impurities are sufficiently removed during the conversion of graphite to RGOs and that they have little or no effect on the final material's properties. On the contrary, metallic impurities inherent in the parent graphite are retained in the resultant chemically reduced graphenes at levels widely considered to be trace and negligible but still enough to exert significant influence on the electrochemical responses of RGOs (29). Thus, proper quantification of the metallic impurities present in RGOs is paramount to ensure that the levels of contamination do not have adverse impacts on a specific use for which an RGO is intended. Unfortunately, this characterization is almost always never performed, despite the potential consequences. This situation is reminiscent of the state of carbon nanotube (CNT) research about a decade ago, during which many groundbreaking properties, such as electrocatalytic effects, were initially ascribed to CNTs; these properties were later proven to arise from the presence of residual metallic catalyst impurities within them. The dominant effects of metallic impurities in CNT have been extensively documented in many areas, including electrocatalysis (30–35), toxicity studies (36, 37), and

Significance

Graphene is well-poised to revolutionize many industries because of its multitude of exceptional properties. Current bulk synthesis of graphene materials typically starts with the oxidation of graphite to graphite oxide followed by a reduction step. Many different methods exist for both the oxidation and reduction steps, leading to highly variable types and amounts of metallic contaminations that originate from the reagents themselves. These impurities are able to alter the graphene materials' properties significantly, which impacts the range of potential applications for which these graphene materials are suitable. Thus, proper characterization of metallic contamination is highly important to ensure the suitability of a chosen set of synthetic procedures to the final application of the graphene material.

Author contributions: C.H.A.W. and M.P. designed research; C.H.A.W., Z.S., M.K., J.K., and S.M. performed research; M.K., J.K., and S.M. contributed new reagents/analytic tools; C.H.A.W., Z.S., M.K., J.K., S.M., and M.P. analyzed data; and C.H.A.W. and M.P. wrote the paper.

The authors declare no conflict of interest.

This article is a PNAS Direct Submission.

[1]To whom correspondence should be addressed. Email: pumera.research@gmail.com.

This article contains supporting information online at www.pnas.org/lookup/suppl/doi:10.1073/pnas.1413389111/-/DCSupplemental.

sorption properties of CNTs (38). In the case of CNTs, metallic impurities observed were remnants of catalyst nanoparticles, the presence of which was crucial for successful growth of CNTs. These impurities ultimately proved difficult to remove from the CNT materials (39, 40). For graphene materials prepared from graphite, it is generally assumed that the final graphene materials are free from metallic impurities, because no catalyst is used; otherwise, the impurities originate from inclusions in the starting graphite (28). Herein, we show that ultrapure-certified graphite is contaminated to varying extents by the chemical agents used during synthetic processing to RGO by comprehensively studying the metallic impurity contamination levels in several RGOs synthesized using a combination of the most commonly used procedures in the literature today. The materials are analyzed at each stage of synthesis (i.e., before oxidation, after oxidation, and after reduction), thereby revealing how different routes of synthesis affect the metallic element concentrations (Scheme 1). We show that contamination occurs during the oxidation and reduction procedures themselves at levels significant enough to alter the electrochemical behavior of RGOs, thus highlighting the importance of proper characterization of metal impurities. The origin of many of these metallic elements can be traced back to the oxidizing and reducing agents used during synthesis, with important implications on the potential applications for which RGOs are slated.

Results and Discussion

It has been shown that even trace amounts of metallic impurities originating from the starting graphite are able to influence the electrochemical responses of RGOs (29). To minimize this effect, we used nuclear reactor-grade graphite as the starting material because of its extremely high purity. Neutron activation analysis (NAA) was used as the primary method to determine the levels of impurities present in our materials because of its accuracy and robustness (41). Additionally, because the materials being studied can be irradiated directly, true bulk analysis of the material can be performed as well as elimination of the possibility of contamination during sample preparation for analysis (42). Although the amount of metallic impurities in the nuclear graphite was zero according to the enclosed inductively coupled plasma mass spectrometry (ICP-MS) certification, NAA of the graphite detected the presence of six trace metals, four of which had a concentration well below 1 ppm by mass (Table 1). The NAA data as well as ICP-MS certification confirmed our starting graphite's high purity and also served as a basis for assessing changes in metal concentrations after subsequent oxidation and reduction procedures.

To study the evolution of metallic impurities content incorporated during the synthetic procedures, GO was first prepared using a modified Hummers method, which is the most common oxidation method currently used for GO production. This procedure eliminated most of the original metallic impurities in the starting graphite; however, trace amounts of seven new metals and two metalloids were observed (a total of 11 metallic elements). Hereafter, metals and metalloids will be collectively referred to as metallic elements. Additionally, the concentration of manganese increased drastically from 0.14 to 2,290 ppm (Table 1). Indeed, the Hummers method is known to result in considerable amounts of residual manganese because of the use of permanganate oxidant (43–45). This Hummers GO (HU-GO) was subsequently reduced to yield RGOs (HU-RGOs) using three different methods: thermal treatment (HU-TRGO), sodium borohydride (HU-$NaBH_4$), and hydrazine (HU-N_2H_4). An abundance of Mn-based impurities was observed in the resultant materials as well, with HU-TRGO showing the highest Mn content (5,700 ppm), whereas the Mn concentrations in HU-$NaBH_4$ and HU-N_2H_4 were 3,800 and 3,000 ppm Mn, respectively. Our group has shown previously that Mn-based impurities exert influence on the electrocatalysis of the oxygen

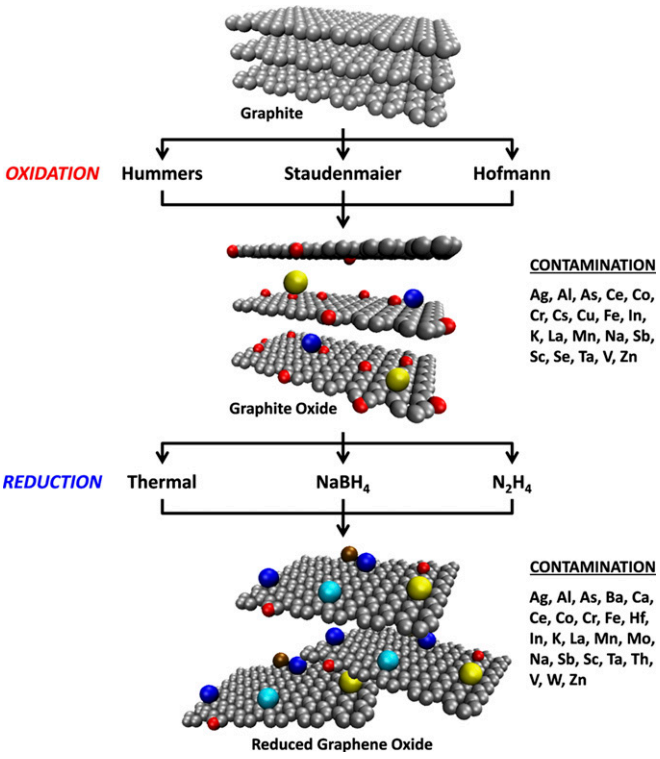

Scheme 1. Common synthesis methods for the preparation of RGOs using graphite as a starting material, which ultimately leads to varying contamination arising from impurities within the chemical agents used. Gray spheres represent carbon atoms, red spheres represent oxygen atoms, and other colors represent metallic impurities.

reduction reaction at carbon electrode surfaces (46). We verified this phenomenon once again by recording linear sweep voltammograms of glassy carbon (GC) electrodes modified with HU-RGOs in the presence of air-saturated KOH, with an unmodified GC electrode serving as a representation of noncatalytic response (Fig. 1). The oxygen reduction onset potential at the noncatalytic bare GC electrode was at −265 mV. The onset potential on HU-RGO–modified GC electrodes was clearly shifted toward more positive potentials, with HU-TRGO showing the largest shift (onset potential of −121 mV) as a result of its high Mn concentration. A similar but slightly less positive value (−135 mV) was noted for HU-N_2H_4. Comparatively, the onset potential at the MnO_2-modified electrode was −92 mV. Intriguingly, the corresponding onset potential for HU-$NaBH_4$ was −226 mV, despite possessing a higher Mn content than HU-N_2H_4. This decreased catalytic activity is most likely due to the relative inefficiency of borohydride reduction and exfoliation compared with thermal treatment and hydrazine. SEM (Fig. S1) showed that HU-$NaBH_4$ existed primarily as large areas of stacked sheets, which is in contrast to the highly exfoliated wrinkled structures seen in HU-TRGO and HU-N_2H_4. This morphology is consistent with other studies, in which the surface areas of $NaBH_4$-reduced RGOs are distinctly lower than that of hydrazine-reduced RGOs (20, 47–49). As a result, a large proportion of the Mn-based impurities in HU-$NaBH_4$ would have been sheathed in between these stacked sheets, rendering them surface-inaccessible and thus, leading to the greatly reduced catalytic effect observed.

Although the incorporation of manganese-based impurities was expected because of the use of permanganate oxidant, contamination with elements not typically associated with the synthesis process was also observed. In addition to residual Na,

Table 1. Elemental concentrations of metals and metalloids (ppm by mass) present in graphite, HU-GO, and HU-RGOs and their expanded uncertainties (coverage factor $k = 2$) as determined by NAA

	Elemental concentration (ppm)				
Element	Graphite	HU-GO	HU-TRGO	HU-$NaBH_4$	HU-N_2H_4
Ag	<0.12	<0.06	<0.11	2.22 ± 0.17	1.90 ± 0.17
Al	5.2 ± 1.6	<60	<110	310 ± 70	420 ± 80
As	<0.03	0.056 ± 0.012	1.08 ± 0.12	<1	<17
Ba	<3	<7	<9	19 ± 5	570 ± 40
Ce	<0.3	<0.1	<0.3	5.9 ± 0.4	1.20 ± 0.17
Co	<0.01	0.157 ± 0.013	6.2 ± 0.4	2.17 ± 0.16	1.42 ± 0.10
Cr	<0.4	1.82 ± 0.15	50 ± 4	5.2 ± 0.4	9.2 ± 0.7
Cs	<0.03	0.028 ± 0.008	<0.15	<0.03	<0.05
Cu	<1.2	130 ± 40	<200	<200	<400
Fe	<18	82 ± 6	270 ± 20	123 ± 12	144 ± 16
Hf	<0.03	<0.01	0.055 ± 0.014	0.33 ± 0.05	0.26 ± 0.02
In	0.016 ± 0.002	<0.1	<0.8	0.63 ± 0.12	1.97 ± 0.14
K	<30	820 ± 60	2,410 ± 180	<1,400	<10,000
La	0.031 ± 0.004	<0.004	<0.3	<0.15	<2
Mn	0.14 ± 0.02	2,290 ± 160	5,700 ± 400	3,800 ± 300	3,000 ± 200
Na	1.0 ± 0.3	96 ± 7	138 ± 10	7,600 ± 500	420 ± 70
Sb	<0.009	0.012 ± 0.003	<0.3	0.068 ± 0.016	0.37 ± 0.04
Sc	<0.002	0.0017 ± 0.0004	0.011 ± 0.001	0.021 ± 0.002	0.024 ± 0.002
Ta	<0.013	<0.006	0.26 ± 0.02	0.066 ± 0.006	0.038 ± 0.004
Th	<0.04	<0.013	<0.03	0.059 ± 0.013	<0.04
V	0.059 ± 0.014	<1.8	<5	<5	9 ± 2
Zn	<0.8	<150	3.0 ± 0.8	114 ± 8	169 ± 12

Values below the detection limit of the NAA procedure are also shown. These values and to a lesser extent, the uncertainties vary as a function of the matrix composition, including nonmetal and nonmetalloid elements.

K, and Mn as expected because of the use of potassium permanganate and sodium nitrate during the oxidation procedure, new metallic elements (As, Co, Cr, Cs, Cu, Fe, Sb, and Sc) were also introduced into the HU-GO sample after the oxidative treatment. The origin of most of these elements is likely to be the synthesis reagents themselves; ICP-optical emission spectrometry (OES) of $KMnO_4$ and $NaNO_3$ showed the presence of eight metallic elements (Ca, Co, Cr, Cu, Fe, Ni, Pb, and Zn), which are seen in Table S1. Similarly, the three reductive processes subsequently used to obtain HU-RGOs introduced three to nine new trace metallic impurities depending on the reduction method used (Table 1). The concentrations of certain metals also increased postreduction. For example, iron concentrations within HU-TRGO, HU-$NaBH_4$, and HU-N_2H_4 were determined to be 270, 123, and 144 ppm, respectively, whereas there was 82 ppm Fe in HU-GO (no Fe was detected in the starting graphite).

To determine whether these Fe impurities would influence the electrochemical properties of HU-RGOs, we used cumene hydroperoxide (CHP) as a molecular probe, which is known to undergo catalytic reduction in the presence of iron (29). As can be seen from the cyclic voltammograms in Fig. 2, the noncatalytic reduction of CHP occurs on a bare GC electrode, giving rise to a reduction peak in the region of −830 mV. For GC electrodes modified with HU-RGOs, we noted a trend of increasing shift in reduction potential with increasing Fe content. The electrode modified with HU-TRGO (highest Fe content) exhibited a reduction peak drastically shifted to −457 mV, whereas those of HU-N_2H_4 (second highest) and HU-$NaBH_4$ (lowest) were −566 and −606 mV, respectively. For comparison, the catalytic reduction of CHP by Fe_3O_4 nanoparticles was found to occur at −496 mV, which is in the same region as HU-TRGO. Hence, it is evident that different reduction procedures (encompassing both thermal and chemical means) unintentionally introduce different amounts of trace Fe impurities into HU-RGOs, with varying influence on their electrochemical properties dependent on the level of contamination.

Along with the above results, we sought to investigate the changes in impurities contents originating from the oxidation procedure itself by using two other oxidation procedures (the Staudenmaier methods and Hofmann method) to first synthesize two other GOs [Staudenmaier GO (ST-GO) and Hofmann GO (HO-GO), respectively] and then use a uniform reduction procedure. NAA of ST-GO revealed 11 different trace metallic elements, which is numerically similar to those in HU-GO, although the identities of several

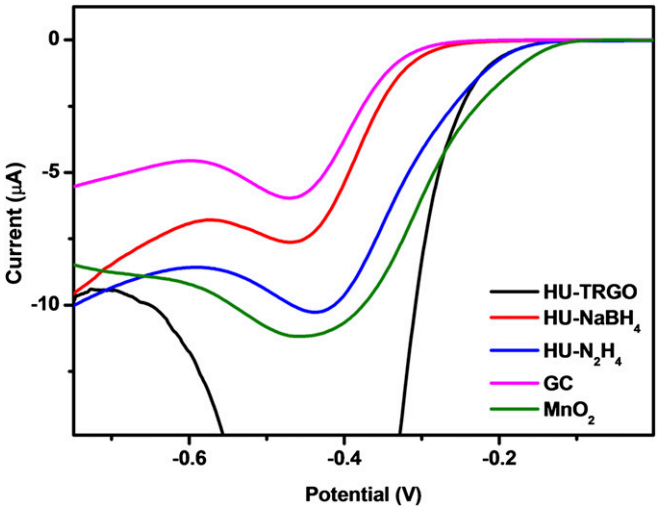

Fig. 1. Linear sweep voltammograms for air-saturated 0.1 M KOH on HU-RGO–modified GC electrodes, as well as comparative voltammograms for bare and MnO_2-modified GC electrodes.

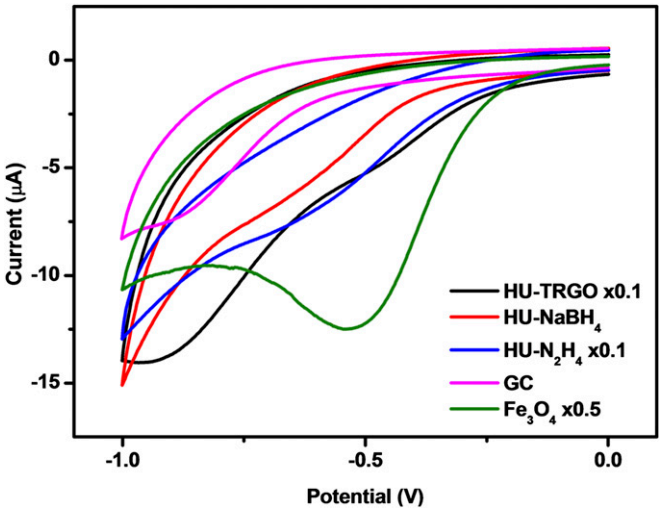

Fig. 2. Cyclic voltammograms for 10 mM CHP on HU-RGO–modified GC electrodes, as well as comparative voltammograms for bare and Fe_3O_4-modified GC electrodes. The suffix × denotes the number of times the current values of the cyclic voltammograms were scaled for ease of comparison.

elements were different (Table 2). HO-GO had the highest contamination with a total of 15 metallic elements. The decreased amounts (both in terms of types as well as concentrations) of impurities in ST-GO compared with HO-GO can be attributed to the use of fuming nitric acid in the Staudenmaier method, which is much more corrosive and thus, better able to remove metallic impurities than the concentrated nitric acid used in the Hofmann method.

A standard thermal reduction was then applied to ST-GO, HU-GO, and HO-GO to obtain ST-TRGO, HU-TRGO, and HO-TRGO, respectively. Thermal reduction was chosen because this procedure was found to introduce the least amount of new trace impurities into the HU-RGOs studied above. This result can be understood to occur because thermal reduction does not require any additional solution processing, thus eliminating additional contamination from reagents and experimental workup. NAA of the TRGOs (Tables 1 and 2) showed that thermal reduction of the GOs resulted in a general increase in the concentrations of metallic elements of around an order of magnitude, with only slight differences in the identities of metallic contaminants. On the basis of NAA measurements, the widest range of contamination from metallic elements was found in ST-TRGO. However, unlike the previous case, in which the NAA detection limits in HU-RGOs were similar regardless of reduction method, the detection limits for certain elements in ST-TRGO, HU-TRGO, and HO-TRGO showed much larger variance. For example, the detection limit of nickel using NAA ranged from 800 ppm in ST-TRGO to 20,000 ppm in HU-TRGO; these detection limits are also far too high for meaningful trace detection of Ni-based impurities. Consequently, ICP-OES was also carried out on the TRGOs, which obtained Ni concentrations of 7.0, 14.0, and 20.6 ppm in ST-TRGO, HU-TRGO, and HO-TRGO, respectively. Once again, the origin of these nickel impurities can be traced back to the reagents used during synthesis (Table S1). Nickel-based substrates have been shown to play a pivotal role in the electrocatalytic oxidation of hydrazine, sometimes in tandem with iron compounds (50–52). Cyclic voltammograms of a bare GC electrode (noncatalytic) in the presence of hydrazine showed a small oxidation wave beginning at +151 mV (Fig. 3). In contrast, distinctly earlier oxidation waves were noted for the TRGO-modified electrodes, with onset potentials correlated to Ni content (+100, +64, and +53 mV for ST-TRGO, HU-TRGO, and HO-TRGO, respectively) and similar to the response shown by NiO-modified electrodes (+65 mV).

The results discussed above indisputably show that metallic impurities are introduced during both oxidation and reduction procedures in the synthesis of RGOs and that the identities of the impurities are not easily anticipated unless thorough elemental analyses on the materials as well as reagents are carried out. Although we have only examined how these metallic impurities can impact the electrochemical responses of RGOs, it is important to keep in mind that other properties can be affected as well. For metallic elements with higher levels of contamination, potassium doping is known to have profound effects on the electronic properties of graphene (53, 54), whereas the presence of aluminum on graphene greatly increases its affinity for gases, such as N_2O and CO (55, 56). Additionally, graphene films have been envisaged to function as water desalination systems because of the potential of tuning pore sizes to allow permeation or rejection of different ions (57). However, the leaching of impurities from within the graphene membrane itself may be a potential problem, considering that the World Health Organization guideline values for chromium and arsenic in drinking water are a mere 50 and 10 parts per billion, respectively (58). We also emphasize our use of exceedingly pure graphite as the starting material in this work to exclude the contribution of contamination from inherent impurities. In reality, the synthesis of RGOs typically uses natural or synthetic graphite, which is more economically feasible. Unfortunately, these graphites possess far higher levels of initial metallic contamination (which remain in significant amounts even after purification), thus compounding the issues highlighted.

Conclusion

We have tracked the changes in the concentrations of metallic elements present in several graphene materials at each stage of synthesis; these materials were prepared using three different oxidation methods as well as three different reduction methods. The synthetic procedures were found to vary significantly in terms the types of impurities introduced as well as the extent of contamination, and the origin of these metallic elements can be traced back to the reagents used for oxidation and reduction of the materials involved. These impurities are highly active in the catalysis of an array of electrochemical reactions, being able to dramatically alter the electrochemical responses of

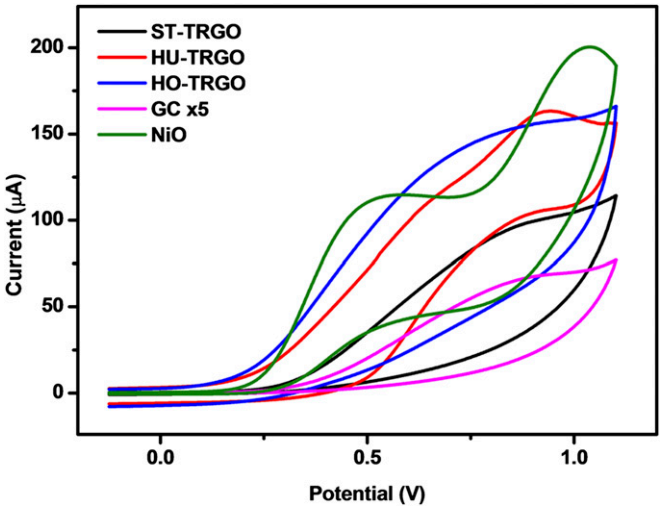

Fig. 3. Cyclic voltammograms for 5 mM hydrazine on TRGO-modified GC electrodes as well as comparative voltammograms for bare and NiO-modified GC electrodes. The suffix x denotes the numbers of times that the current values of the cyclic voltammograms were scaled for ease of comparison.

Table 2. Elemental concentrations of metals and metalloids (ppm by mass) present in ST-GO, ST-TRGO, HO-GO, and HO-TRGO and their expanded uncertainties (coverage factor $k = 2$) as determined by NAA

	Elemental concentration (ppm)			
Element	ST-GO	ST-TRGO	HO-GO	HO-TRGO
Ag	0.038 ± 0.011	<0.12	<0.03	<0.5
Al	<4	57 ± 5	<12	<150
As	0.60 ± 0.06	0.83 ± 0.09	<0.06	<0.1
Ca	<50	4,500 ± 1600	<30	<7
Ce	<0.06	<0.4	2.5 ± 0.3	<0.9
Co	0.058 ± 0.005	8.1 ± 0.8	0.33 ± 0.02	1.49 ± 0.11
Cr	0.94 ± 0.08	69 ± 5	0.72 ± 0.08	42 ± 3
Cs	<0.005	<0.05	0.188 ± 0.004	<0.08
Fe	8.3 ± 1.5	340 ± 30	16 ± 4	260 ± 30
In	<0.02	0.153 ± 0.013	0.013 ± 0.004	0.076 ± 0.016
K	360 ± 30	60 ± 20	240 ± 20	450 ± 100
La	<0.008	<0.1	0.022 ± 0.004	0.080 ± 0.016
Mn	0.62 ± 0.06	5.9 ± 0.4	3.1 ± 0.2	97 ± 7
Mo	<0.6	4.4 ± 0.8	<0.6	<7
Na	3.5 ± 0.3	31 ± 2	12.1 ± 0.9	44 ± 4
Pt	<0.6	<5	<0.6	75 ± 6
Sb	0.042 ± 0.004	0.19 ± 0.02	0.040 ± 0.006	0.12 ± 0.03
Sc	<0.01	<0.004	0.0015 ± 0.0002	<0.007
Se	0.34 ± 0.03	<0.4	<0.14	<1
Ta	<0.003	<0.06	0.019 ± 0.004	<0.1
V	<0.12	18.2 ± 1.3	0.37 ± 0.07	2.6 ± 0.3
W	<0.07	3.7 ± 0.3	<0.07	<1
Zn	0.69 ± 0.11	3.5 ± 1.1	2.0 ± 0.2	<6

Values below the detection limit of the NAA procedure are also shown. These values and to a lesser extent, the uncertainties vary as a function of the matrix composition, including nonmetal and nonmetalloid elements.

RGOs as shown in our investigations. Because metallic impurities are able to affect many other properties of graphene materials, their implications are wide-reaching, potentially impacting many proposed applications of graphene materials.

Methods

Synthesis of Graphene Oxides. Graphene oxides were synthesized according the Staudenmaier (14), Hofmann (15, 16), and Hummers (17) methods. Detailed procedures are in *SI Methods*.

Thermal Reduction of GO. GOs prepared using the procedures above were subjected to thermal reduction/exfoliation at 1,000 °C; 0.1 g GO was placed into a porous quartz glass capsule connected to a magnetic manipulator inside a vacuum tight tube furnace with controlled atmosphere. The magnetic manipulator is capable of creating a temperature gradient over 1,000 °C min^{-1}. The reactor was then flushed with nitrogen gas by repeated evacuation of the tube furnace to remove any traces of oxygen, then quickly inserted by the magnetic manipulator to a preheated furnace, and held in the furnace for 12 min. The flow of nitrogen (99.9999% purity) during the exfoliation procedure was 1,000 mL min^{-1} to remove any byproducts from the procedure.

Sodium Borohydride Reduction of GO. GO prepared using the Hummers method (500 mg) was dispersed in 500 mL deionized water by ultrasonication (400 W for 30 min). The suspension was alkalized to pH 10 with 1 M NaOH, and 5 g $NaBH_4$ was added to the suspension. The reaction mixture was heated at 80 °C with vigorous stirring for 1 h. The reaction mixture was allowed to cool to room temperature, after which the RGO was separated by suction filtration, repeatedly washed with deionized water, and dried in a vacuum oven at 50 °C for 48 h.

Hydrazine Reduction of GO. GO prepared using the Hummers method (500 mg) was dispersed in 500 mL deionized water by ultrasonication (400 W for 30 min). The suspension was alkalized to pH 10 with 1 M KOH, and 5 mL hydrazine hydrate was added to the suspension. The reaction mixture was heated under reflux for 24 h. After cooling down to room temperature, the RGO was separated by suction filtration, repeatedly washed with deionized water, and dried in a vacuum oven at 50 °C for 48 h.

Characterization of Materials by NAA, ICP-OES, SEM, and Voltammetry. Samples of nuclear graphite, GOs, and RGOs prepared by various procedures were packed for irradiation into disk-shaped polyethylene capsules with a 25-mm diameter made by sealing of polyethylene foils with 0.2-mm thickness. Irradiations were carried out in the LVR-15 experimental reactor of the Research Centre Řež, Ltd. within the Center of Accelerators and Nuclear Analytical Methods infrastructure (Ministry of Education, Youth and Sports of the Czech Republic Project No. 2011019). Short-time irradiations (1 min) were carried out in channel H1 using a pneumatic transport system with a transport time of 3.5 s. Long-time irradiations were done in channel H8 for 3 h. Thermal neutron fluence rates in both channels were 3–4 × 10^{13} cm^{-2} s^{-1}. For k_0 standardization, the bare triple-monitor method (59) was used for determination of neutron flux parameters in the irradiation channels. For this purpose, newly developed monitors for short- (60) and long-time irradiations (61) were used. γ-rRay spectra of samples and monitors were measured with coaxial high-purity germanium detectors (relative efficiency = 21–78%, full width at half maximum resolution = 1.80–1.85 keV, both for the 1,332.5 keV photons of ^{60}Co) interfaced to a Canberra Genie 2000 γ-spectrometer. Decay times, counting times, and counting geometry were selected according to sample activities and half-lives of radionuclides present to optimize detection limits of as many elements as possible. The measurements were evaluated with the Kayzero for Windows software package. For verification of results, standard reference materials of the US National Institute of Standards and Technology (NIST SRMs), namely NIST SRM 1547 Peach Leaves, NIST SRM 2711 Montana Soil, and NIST SRM 1633b Coal Fly Ash, were coanalyzed with the samples and showed excellent agreement with the NIST certified values. The difference between matrix composition of the materials in this study and that of NIST SRMs does not invalidate the proof of accuracy because of matrix independence of NAA.

ICP-OES measurements were performed with Spectro ARCOS (SPECTRO Analytical Instruments). The spectrometer used the Paschen–Runge configuration with an optimized Rowland circle polychromator, measuring simultaneously in the broad spectral range of 130–770 nm using 32 linear CCD detectors. The detection limits are at ppb (by mass) levels for the elements determined.

For graphite and graphene sample decomposition, a procedure based on Schöniger oxidation was used (62). A precisely weighted sample of 5 mg was wrapped in ash-free nitrocellulose paper and burned in a flask (filled with pure oxygen) with Pt sample holder. The burning products were decomposed by prolonged ultrasonication and heating with ICP-grade nitric acid. After this procedure, the sample solution was diluted with deionized water ($R = 18.2$ MΩ) to obtain a concentration of nitric acid of around 1% and used for analysis. Blank experiments were performed with ash-free cellulose paper to subtract the amount of impurities introduced by sample preparation. The calibration of the spectrometer was performed with certified ICP-OES elements standards in 2% (wt/wt) HNO_3 and 2% (wt/wt) HNO_3–2% (wt/wt) HCl matrixes; Y was used as an internal standard.

A JEOL 7600F Field-Emission Scanning Electron Microscope (JEOL) was used to acquire the SEM images at 5.0 kV and a working distance of 5.7 mm. The solid samples were immobilized onto a carbon tape on an aluminum SEM holder for analyses.

Voltammetry experiments were carried out on a μAutolab Type III Electrochemical Analyzer (Eco Chemie) connected to a personal computer and controlled by General Purpose Electrochemical Systems, version 4.9 software (Eco Chemie). Electrochemical experiments were carried out in a 5-mL electrochemical cell at room temperature with a three-electrode configuration (Ag/AgCl as the reference and Pt as the auxiliary). Linear sweep voltammetry experiments were conducted at a scan rate of 100 mV s^{-1} with 10 mM air-saturated KOH as the analyte. Cyclic voltammetry experiments were conducted at a scan rate of 100 mV s^{-1} with 10 mM CHP or 5 mM hydrazine as the molecular probes in a supporting electrolyte of 50 mM phosphate buffer solution (pH 7.4). All electrochemical potentials in this paper are stated vs. the Ag/AgCl reference electrode. GC electrode surfaces were renewed before each measurement or modification by polishing for 2 min on a polishing pad with alumina slurry and then washed with deionized water of resistivity not less than 18.2 MΩ cm (Milli-Q; Millipore).

Suspensions of graphene materials and metal oxide nanoparticles were prepared with a concentration of 1 mg mL^{-1} in *N,N*-dimethylformamide with 30 min sonication. Modification of GC electrode surfaces with these materials was performed by depositing a 1-μL aliquot of the suspension onto the electrode, after which the solvent was evaporated under a sun lamp for 20 min. The suspensions were sonicated for an additional 1 min before each deposition to ensure homogeneity.

ACKNOWLEDGMENTS. M.K. and J.K. were supported by Czech Science Foundation Grant P108/12/G108. Z.S. was supported by Specific University Research Grant MSMT 20/2014. M.P. acknowledges Ministry of Education, Singapore Tier 2 Grant MOE2013-T2-1-056; ARC 35/13.

1. Geim AK, Novoselov KS (2007) The rise of graphene. *Nat Mater* 6(3):183–191.
2. Novoselov KS, et al. (2004) Electric field effect in atomically thin carbon films. *Science* 306(5696):666–669.
3. Pumera M (2010) Graphene-based nanomaterials and their electrochemistry. *Chem Soc Rev* 39(11):4146–4157.
4. Gomez De Arco L, et al. (2010) Continuous, highly flexible, and transparent graphene films by chemical vapor deposition for organic photovoltaics. *ACS Nano* 4(5):2865–2873.
5. Pumera M (2010) Graphene-based nanomaterials and their electrochemistry. *Energy Environ Sci* 4(3):668–674.
6. Stoller MD, Park S, Zhu Y, An J, Ruoff RS (2008) Graphene-based ultracapacitors. *Nano Lett* 8(10):3498–3502.
7. Stankovich S, et al. (2006) Graphene-based composite materials. *Nature* 442(7100): 282–286.
8. Liu Z, Robinson JT, Sun X, Dai H (2008) PEGylated nanographene oxide for delivery of water-insoluble cancer drugs. *J Am Chem Soc* 130(33):10876–10877.
9. Feng L, Liu Z (2011) Graphene in biomedicine: Opportunities and challenges. *Nanomedicine (Lond)* 6(2):317–324.
10. Rogers JA (2008) Electronic materials: Making graphene for macroelectronics. *Nat Nanotechnol* 3(5):254–255.
11. IUPAC (1997) *Compendium of Chemical Terminology (The "Gold Book")* (Blackwell, Oxford), 2nd Ed.
12. Lee S, Eom SH, Chung JS, Hur SH (2013) Large-scale production of high-quality reduced graphene oxide. *Chem Eng J* 233:297–304.
13. Brodie BC (1859) On the atomic weight of graphite. *Philos Trans R Soc Lond B Biol Sci* 149:249–259.
14. Staudenmaier L (1898) Verfahren zur Darstellung der Graphitsäure. *Ber Dtsch Chem Ges* 31(2):1481–1487.
15. Hofmann U, König E (1937) Untersuchungen über Graphitoxyd. *Z Anorg Allg Chem* 234(4):311–336.
16. Hofmann U, Holst R (1939) Über die Säurenatur und die Methylierung von Graphitoxyd. *Ber Dtsch Chem Ges* 72(4):754–771.
17. Hummers WS, Jr, Offeman RE (1958) Preparation of graphitic oxide. *J Am Chem Soc* 80(6):1339.
18. Zhou M, et al. (2009) Controlled synthesis of large-area and patterned electrochemically reduced graphene oxide films. *Chemistry* 15(25):6116–6120.
19. Kumar P, Subrahmanyam KS, Rao CNR (2011) Graphene produced by radiation-induced reduction of graphene oxide. *Int J Nanosci Ser* 10(04n05):559–566.
20. Stankovich S, et al. (2007) Synthesis of graphene-based nanosheets via chemical reduction of exfoliated graphite oxide. *Carbon* 45(7):1558–1565.
21. Shin HJ, et al. (2009) Efficient reduction of graphite oxide by sodium borohydride and its effect on electrical conductance. *Adv Funct Mater* 19(12):1987–1992.
22. Ambrosi A, Chua CK, Bonanni A, Pumera M (2012) Lithium aluminum hydride as reducing agent for chemically reduced graphene oxides. *Chem Mater* 24(12): 2292–2298.
23. Zhu C, Guo S, Fang Y, Dong S (2010) Reducing sugar: New functional molecules for the green synthesis of graphene nanosheets. *ACS Nano* 4(4):2429–2437.
24. Wang Y, Shi Z, Yin J (2011) Facile synthesis of soluble graphene via a green reduction of graphene oxide in tea solution and its biocomposites. *ACS Appl Mater Interfaces* 3(4):1127–1133.
25. Chua CK, Pumera M (2014) Chemical reduction of graphene oxide: A synthetic chemistry viewpoint. *Chem Soc Rev* 43(1):291–312.
26. Hu FM, Ma T, Lin H-Q, Gubernatis JE (2011) Magnetic impurities in graphene. *Phys Rev B Condens Matter* 84(7):075414.
27. Krasheninnikov AV, Nieminen RM (2011) Attractive interaction between transition metal atom impurities and vacancies in graphene: A first-principles study. *Theor Chem Acc* 129(3-5):625–630.
28. Ambrosi A, et al. (2012) Metallic impurities in graphenes prepared from graphite can dramatically influence their properties. *Angew Chem Int Ed Engl* 51(2):500–503.
29. Ambrosi A, et al. (2012) Chemically reduced graphene contains inherent metallic impurities present in parent natural and synthetic graphite. *Proc Natl Acad Sci USA* 109(32):12899–12904.
30. Sljukić B, Banks CE, Compton RG (2006) Iron oxide particles are the active sites for hydrogen peroxide sensing at multiwalled carbon nanotube modified electrodes. *Nano Lett* 6(7):1556–1558.
31. Banks CE, Crossley A, Salter C, Wilkins SJ, Compton RG (2006) Carbon nanotubes contain metal impurities which are responsible for the "electrocatalysis" seen at some nanotube-modified electrodes. *Angew Chem Int Ed Engl* 45(16):2533–2537.
32. Batchelor-McAuley C, Wildgoose GG, Compton RG, Shao L, Green MLH (2008) Copper oxide nanoparticle impurities are responsible for the electroanalytical detection of glucose seen using multiwalled carbon nanotubes. *Sens Actuators B Chem* 132(1): 356–360.
33. Dai X, Wildgoose GG, Compton RG (2006) Apparent 'electrocatalytic' activity of multiwalled carbon nanotubes in the detection of the anaesthetic halothane: Occluded copper nanoparticles. *Analyst (Lond)* 131(8):901–906.
34. Ambrosi A, Pumera M (2010) Regulatory peptides are susceptible to oxidation by metallic impurities within carbon nanotubes. *Chemistry* 16(6):1786–1792.
35. Pumera M, Ambrosi A, Chng ELK (2012) Impurities in graphenes and carbon nanotubes and their influence on the redox properties. *Chem Sci* 3:3347–3355.
36. Guo L, et al. (2007) Iron bioavailability and redox activity in diverse carbon nanotube samples. *Chem Mater* 19(14):3472–3478.
37. Liu X, et al. (2007) Bioavailability of nickel in single-wall carbon nanotubes. *Adv Mater* 19(19):2790–2796.
38. Tian X, et al. (2010) Metal impurities dominate the sorption of a commercially available carbon nanotube for Pb(II) from water. *Environ Sci Technol* 44(21):8144–8149.
39. Hou P-X, Liu C, Cheng H-M (2008) Purification of carbon nanotubes. *Carbon* 46(15): 2003–2025.
40. Pumera M (2007) Carbon nanotubes contain residual metal catalyst nanoparticles even after washing with nitric acid at elevated temperature because these metal nanoparticles are sheathed by several graphene sheets. *Langmuir* 23(11):6453–6458.
41. International Union of Pure and Applied Chemistry (1995) Isotopic and nuclear analytical techniques in biological systems: A critical study. Part IX. Neutron activation analysis. *Pure Appl Chem* 67(11):1929–1941.
42. IAEA (2001) *Use of Research Reactors for Neutron Activation Analysis (IAEA-TECDOC-1215)* (IAEA, Vienna).
43. Panich AM, Shames AI, Aleksenskii AE, Dideikin A (2012) Magnetic resonance evidence of manganese–graphene complexes in reduced graphene oxide. *Solid State Commun* 152(6):466–468.
44. Paratala BS, Jacobson BD, Kanakia S, Francis LD, Sitharaman B (2012) Physicochemical characterization, and relaxometry studies of micro-graphite oxide, graphene nanoplatelets, and nanoribbons. *PLoS ONE* 7(6):e38185.
45. Panich AM, Shames AI, Sergeev NA (2013) Paramagnetic impurities in graphene oxide. *Appl Magn Reson* 44(1-2):107–116.
46. Wang L, Ambrosi A, Pumera M (2013) "Metal-free" catalytic oxygen reduction reaction on heteroatom- doped graphene is caused by trace metal impurities. *Angew Chem Int Ed Engl* 52(51):13818–13821.
47. Kumar R, Suresh VM, Maji TK, Rao CNR (2014) Porous graphene frameworks pillared by organic linkers with tunable surface area and gas storage properties. *Chem Commun (Camb)* 50(16):2015–2017.
48. Sil S, Kuhar N, Acharya S, Umapathy S (2013) Is chemically synthesized graphene 'really' a unique substrate for SERS and fluorescence quenching? *Sci Rep* 3:3336.
49. Park S, et al. (2011) Hydrazine-reduction of graphite- and graphene oxide. *Carbon* 49(9):3019–3023.
50. Wong CHA, Chua CK, Khezri B, Webster RD, Pumera M (2013) Graphene oxide nanoribbons from the oxidative opening of carbon nanotubes retain electrochemically active metallic impurities. *Angew Chem Int Ed Engl* 52(33):8685–8688.
51. Adekunle AS, Ozoemena KI (2008) Insights into the electro-oxidation of hydrazine at single-walled carbon-nanotube-modified edge-plane pyrolytic graphite electrodes electro-decorated with metal and metal oxide films. *J Solid State Electrochem* 12(10): 1325–1336.
52. Abbaspour A, Khajehzadeh A, Ghaffarinejad A (2009) Electrocatalytic oxidation and determination of hydrazine on nickel hexacyanoferrate nanoparticles-modified carbon ceramic electrode. *J Electroanal Chem (Lausanne Switz)* 631(1-2):52–57.
53. Ohta T, Bostwick A, Seyller T, Horn K, Rotenberg E (2006) Controlling the electronic structure of bilayer graphene. *Science* 313(5789):951–954.
54. Xue M, et al. (2012) Superconductivity in potassium-doped few-layer graphene. *J Am Chem Soc* 134(15):6536–6539.
55. Lv YA, Zhuang GL, Wang JG, Jia YB, Xie Q (2011) Enhanced role of Al or Ga-doped graphene on the adsorption and dissociation of N_2O under electric field. *Phys Chem Phys* 13(27):12472–12477.
56. Ao ZM, Yang J, Li S, Jiang Q (2008) Enhancement of CO detection in Al doped graphene. *Chem Phys Lett* 461(4-6):276–279.
57. Cohen-Tanugi D, Grossman JC (2012) Water desalination across nanoporous graphene. *Nano Lett* 12(7):3602–3608.
58. WHO (2011) *Guidelines for Drinking-Water Quality* (WHO, Geneva), 4th Ed.
59. De Corte F, Simonits A (1994) *Vade Mecum for k_0 Users* (DMS Research, Geleen, The Netherlands).
60. Kubešová M, Kučera J, Fikrle M (2011) A new monitor set for the determination of neutron flux parameters in short-time k_0-NAA. *Nucl Instrum Methods Phys Res A* 656(1):61–64.
61. Kubešová M, Krausová I, Kučera J (2014) Verification of k_0-NAA results at the LVR-15 reactor in Řež with the use of Au+Mo+Rb(+Zn) monitor set. *J Radioanal Nucl Chem* 300(2):473–480.
62. MacDonald AMG (1961) The oxygen flask method. A review. *Analyst* 86(1018):3–12.